Article

Consideration of Statistical Approaches Within the Accelerated Assessment of Fatigue Properties of Metallic Materials

Fabian Weber [1,2,*], Aline Wagner [1], Janina Koziol [1], Felix Weber [3], Christoph Broeckmann [3] and Peter Starke [1,2]

1   Department of Material Sciences and Materials Testing (WWHK), Institute QM[3], University of Applied Sciences Kaiserslautern, Schoenstr. 11, 67659 Kaiserslautern, Germany; aline.wagner@hs-kl.de (A.W.); janina.koziol@hs-kl.de (J.K.); peter.starke@hs-kl.de (P.S.)
2   Faculty of Natural Sciences and Technology, Saarland University, 66123 Saarbrücken, Germany
3   Institute for Materials Applications in Mechanical Engineering, RWTH Aachen University, 52062 Aachen, Germany; f.weber@iwm.rwth-aachen.de (F.W.); c.broeckmann@iwm.rwth-aachen.de (C.B.)
*   Correspondence: fabian.weber@hs-kl.de; Tel.: +49-(0)-631-3724-2259

Abstract: Understanding the fatigue behaviour of metallic materials is highly important when it comes to a reliable assessment of material degradation as a result of dynamic loading. Because the provision of such data is associated with great testing effort leading to increased time and cost requirements in terms of conventional methods, accelerated lifetime prediction methods are becoming increasingly important. However, the reduced number of fatigue specimens and tests complicates statistical validations of the obtained results. In this contribution, combinatorial approaches are used to estimate both lifetime prediction bands and virtually-determined S-N curves with a reduced number of specimens, displaying the material-related scatter due to microstructural inhomogeneities. In addition, a variable energy dissipation factor based on cyclic deformation curves is presented, which enables evaluation of materials that exhibit more pronounced scatter, for instance cast materials. An in situ evaluation of the cyclic deformation curves is provided via integration of non-destructive testing methods into the testing rig. Unalloyed SAE 1045 steel, low-alloyed 20MnMoNi5-5 steel, and the cast material EN-GJS-1050-6 are investigated in this research, as these materials posses gradually increasing complexity regarding their respective microstructures.

1. Introduction

Fatigue of metallic materials represents one of the most common reasons for failure under mechanical loading; thus, an outright understanding of the fatigue properties of the materials being used is essential when assessing the integrity of components or structures. The design of specimens and components subjected to dynamic loading is conventionally based on the so-called S-N curves, which represent the relationship between the applied load amplitude and the corresponding number of cycles to failure. However, because a fairly high number of fatigue tests (depending on literature, at least 12–24 fatigue specimens) is required to generate an S-N curve, this is a very time consuming and consequently costly process. Therefore, a number of different lifetime prediction methods (LPMs) have been developed in recent research with the aim of providing fatigue data in an accelerated way. These methods are based on a combination of non-destructive testing (NDT)

and conventional destructive testing. Performing material response-related evaluation of fatigue behavior instead of a lifetime-oriented approach leads to a demonstrably higher information content and enables a mechanism-based investigation of the fatigue process. In previous works by Weber et al. [1,2], this correlation was used to develop a new LPM that uses the non-destructively measured material response to dynamic loading as an input to estimate virtual S-N curves based on only one load increase test (LIT). As a result of the drastic reduction in the required number of specimens, it is not possible to achieve sufficient statistical validation of the obtained results; however, because of inhomogeneities within the microstructure and local stress concentrations, the fatigue behavior of metallic materials can be highly influenced by the inherent scatter of the results. As a result of this, the determination of defined failure probabilities is highly important when it comes to safe and reliable component design. Therefore, the aim of the present research is to provide lifetime prediction bands in the context of accelerated fatigue testing, which can enable statistical validation of test results analogously to conventional scatter bands. The MiDAcLife LPM used in this paper is based on the linear damage accumulation according to Palmgren and Miner. Therefore, Section 1.1 contains a brief overview concerning the state-of-the-art of damage accumulation methods. As the aim of this research is to integrate statistical approaches into accelerated fatigue testing in order to close the gap between the reduced amount of specimens and sufficient validation of the results, Section 1.2 explores statistical methods in fatigue testing.

1.1. Damage Accumulation Models

One of the most prominent methods for evaluating material degradation as a result of dynamic loading is the linear damage accumulation according to Palmgren and Miner [3,4], the fundamental relation of which is provided in Equation (1).

$$D_i = \frac{n_i}{N_{f,i}} \tag{1}$$

The induced partial damage D_i is calculated from the number of applied load cycles n_i and the corresponding number of cycles to failure $N_{f,i}$. During the fatigue process, D_i accumulates until a certain threshold value is reached and specimen failure occurs. Limiting the materials to only steels results in a threshold value of 1.

$$D = \sum D_i = \sum \frac{n_i}{N_{f,i}} = 1 \tag{2}$$

In the literature [5], there are three main variants of the Miner rule: the original, elementary, and Haibach rules. Using the elementary Miner rule, no fatigue strength is taken into account within the S-N curve. In contrast, the original Miner rule states that a distinction must be made between two limiting conditions. If the stress amplitude σ_a is above the fatigue strength σ_e of the material, then the relation shown in Equation (3) applies; otherwise, the number of cycles is considered infinite, as shown in Equation (4).

$$\sigma_a \geq \sigma_e : N = N_e \cdot \left(\frac{\sigma_a}{\sigma_e}\right)^{-k} \tag{3}$$

$$\sigma_a < \sigma_e : N = \infty \tag{4}$$

In Equation (3), the k parameter displays the slope of the S-N curve, whereas N_e indicates the limiting number of cycles. Haibach [6] introduced a model that enables the consideration of the fatigue strength as a function of the progressive damage, providing a further modified version of the Miner rule in which a reduced slope is assumed within a

fictitious area. Based on this insight, the previously presented Equation (4) is replaced by the relation according to Equation (5).

$$N_{fictitious} = N_e \cdot \left(\frac{\sigma_a}{\sigma_e}\right)^{-(2k-1)} \tag{5}$$

Despite the simplicity of the previously explained method, the assumption of linearity can lead to significant deviations in the calculated results; thus, many developments in terms of damage accumulation models have been carried out in recent research.

Because the static toughness of a material contains information regarding both strength and plasticity, it is suitable for the determination of material degradation resulting from a fatigue process. As a consequence, Ye et al. [7] introduced a damage parameter that is based on the correlation of the static toughness and the fatigue process. The proposed methodology is built on the assumption that a reduced static toughness indicates the capability to absorb energy inherently as a result of progressive fatigue damage. In the research of [7], the damage parameter D can be estimated according to Equation (6) as a function of the number of cycles to failure N_f and critical cumulative damage after reaching $N_f - 1$ cycles D_{N_f-1}.

$$D = -\frac{D_{N_f-1}}{ln(N_f)} \cdot \left[1 - \frac{N}{N_f}\right] \tag{6}$$

Instead of considering the static toughness of a material, Manson and Halford [8] used the crack length to determine the corresponding damage parameter. However, even if load sequence effects can be taken into account, their method is not able to consider load interaction effects, necessitating further research.

Based on a finite element method, Benkabouche [9] provided an approach that considers both multi-axial loading and load sequence effects in determining the damage evolution. This allows block loading data to be converted into equivalent constant amplitude data by applying the Crossland criterion. In accordance with the findings of [9] and the approaches of [10], the damage parameter can be described by the correlation of Equation (7).

$$D_i = \frac{\sum_i^{eq} - \sigma_{eq}^{i,max}}{\tau_u - \sigma_{eq}^{i,max}} \tag{7}$$

In the above Equation (7), the damage parameter D_i is provided as a function of the damage stress amplitude at the ith load level $\sum_i^{eq}$, the ultimate stress in torsion tests τ_u, and the maximum equivalent stress $\sigma_{eq}^{i,max}$. As increased load amplitudes support crack initiation, which consequently facilitates crack propagation in terms of lower amplitudes, Yu et al. [11] investigated possibilities regarding the integration of load sequence and load interaction effects. An application-related investigation of damage behavior was performed by Aeran et al. [12]. In their research, the aim was to estimate the fatigue life of roller bearings under the consideration of variable loading conditions. To reach this goal, a damage index δ_i was introduced.

When considering the behavior of nonlinear material in damage accumulation models, so-called iso-damage curves are highly important. Therefore, Bjørheim et al. [13] published a differential approach (Equation (8)) based on the finding that an increased number of cycles leads to more pronounced damage in the material.

$$\frac{dD}{D} = q(\sigma, m)\frac{dn}{n} \tag{8}$$

1.2. Statistical Approaches Concerning the Evaluation of Fatigue Properties Regarding Metallic Materials

In statistical evaluations of the fatigue properties of metallic materials, so-called P-S-N curves (fatigue-probabilistic S-N curves) are often considered in the literature. In the research of Ling and Pan [14], a maximum likelihood method was proposed to reduce the testing effort required to obtain P-S-N curves. Comparable strategies for integrating statistical approaches in fatigue testing were presented in [15–17]. While Gioglio and Rossetto [15] used the maximum likelihood method to generate P-S-N curves and a hypothesis test to compare different batches on the basis of two fatigue specimens, Feng et al. [16] extended the maximum likelihood approach to generate strain amplitude–fatigue life curves. Because material inhomogeneities are particularly likely to lead to increased scatter over the lifetime, Tridello et al. [18] presented two methodologies, namely, the likelihood ratio confidence bound and the bootstrap approach, to allow for lifetime assessment of components with defects.

An important part of statistical evaluations involves selecting the respective distribution function. In this respect, Müller et al. [19] examined a variety of test series with regard to the applicability of the log-normal distribution. For this purpose, they applied the Shapiro–Wilk and Anderson–Darling tests. In addition to the log-normal distribution, there are further distribution functions including an additional parameter, such as the three-parameter Weibull distribution function or the $\log(N\text{-}N_0)$-normal distribution function. In the research of Schijve [20], these functions were examined and compared in terms of fit quality.

In the context of this research, lifetime prediction bands were determined using the pearl string method described by Masendorf and Müller [21]. As part of this process, the numbers of cycles to failure are transferred to a virtual load level according to a defined slope, enabling the application of a log-normal distribution function.

2. Materials and Methods

2.1. Materials

Because the scatter of the lifetime is highly influenced by the microstructure, investigations were performed on three different materials of increasing complexity. First, a non-alloyed SAE 1045 (C45E, 1.1191) steel in a normalized condition is investigated, which is characterized by a ferritic–pearlitic microstructure. Second, investigations regarding a low-alloyed 20MnMoNi5-5 (1.6310) steel with a ferritic–bainitic microstructure interspersed with carbides are performed. The size and distribution of the carbides can have a particularly strong influence on the fatigue properties of the material. Final investigations are carried out an a cast iron EN-GJS-1050-6 material with an ausferritic matrix, which is characterized by different damage mechanisms than steels.

The following Tables 1 and 2 summarize the chemical compositions of the materials along with important mechanical properties such as the yield strength R_e, tensile strength R_m, and total elongation A_t, which were determined according to own experimental analyses.

Table 1. Chemical composition in wt.% of the 20MnMoNi5-5 steel, SAE 1045 steel, and EN-GJS-1050-6 cast iron used in this research.

	C	Si	Mn	S	Cr	Mo	Ni
20MnMoNi5-5	0.218	0.246	1.385	0.003	0.076	0.487	0.762
	C	Si	Mn	S	Cr	Mo	Ni
SAE 1045	0.427	0.232	0.742	0.007	0.070	0.020	0.078

Table 1. *Cont.*

	C	Si	Mn	Cu	Mg	Mo	Ni
EN-GJS-1050-6	3.300	2.000	<0.300	0.800	<0.050	<0.330	1.990

Table 2. Mechanical properties considering static loading of the 20MnMoNi5-5 steel, SAE 1045 steel, and EN-GJS-1050-6 cast iron.

20MnMoNi5-5	R_e, MPa	R_m, MPa	A_t, %
	577.6	673.2	25.4
SAE 1045	R_e, MPa	R_m, MPa	A_t, %
	413.0	710.0	23.5
EN-GJS-1050-6	R_e, MPa	R_m, MPa	A_t, %
	736.0	1003	9.3

Microstructural analysis of the materials was carried out on the basis of a digital microscope type Olympus DSX 1000 (EVIDENT Europe GmbH, Hamburg, Germany) as well as a scanning electron microscope type TESCAN CLARA GMU (TESCAN GmbH, Dortmund, Germany) to enable high-resolution examination of the microstructure.

Figure 1 shows the microstructure of the unalloyed SAE 1045 steel. The overview in Figure 1a displays the distinction between the ferritic and pearlitic areas, while Figure 1b provides more detailed insights into the lamellar structure of the pearlite.
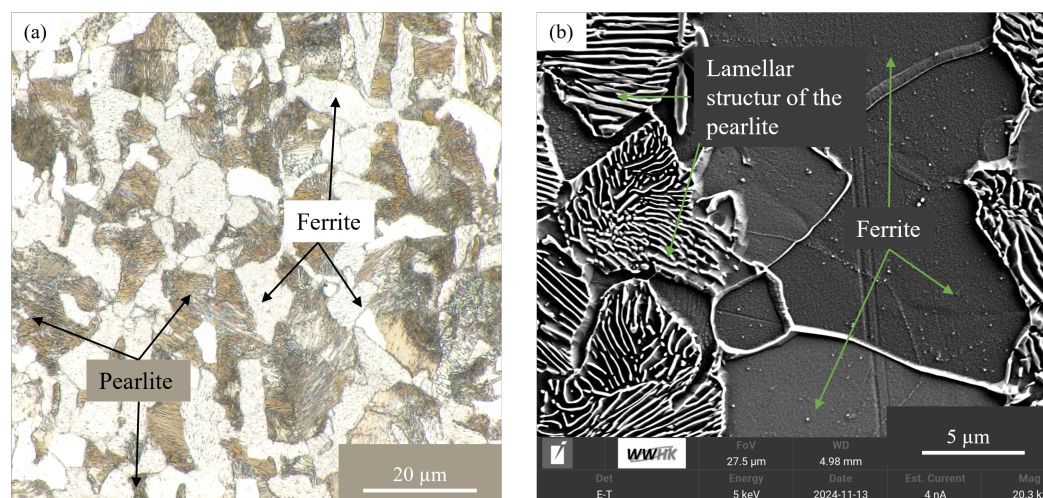

Figure 1. Microstructural analysis of the of the SAE 1045 steel: (**a**) overview of the microstructure based on digital microscopy and (**b**) detailed consideration of the microstructure based on scanning electron microscopy.

In contrast to the microstructure of the SAE 1045 steel in Figure 1, the microstructure of the 20MnMoNi5-5 steel mainly consists of white-colored ferrite areas, as shown in Figure 2a. The arrangement of the carbides, which particularly agglomerate along grain boundaries, evident in Figure 2b. Based on previous research from Haverkamp and Das, it has been proven that these precipitates consist mainly of Fe_3C and M_2C carbides [22–24].

A more extensive description regarding the investigated steel materials can be found in the literature [1,2,25,26].
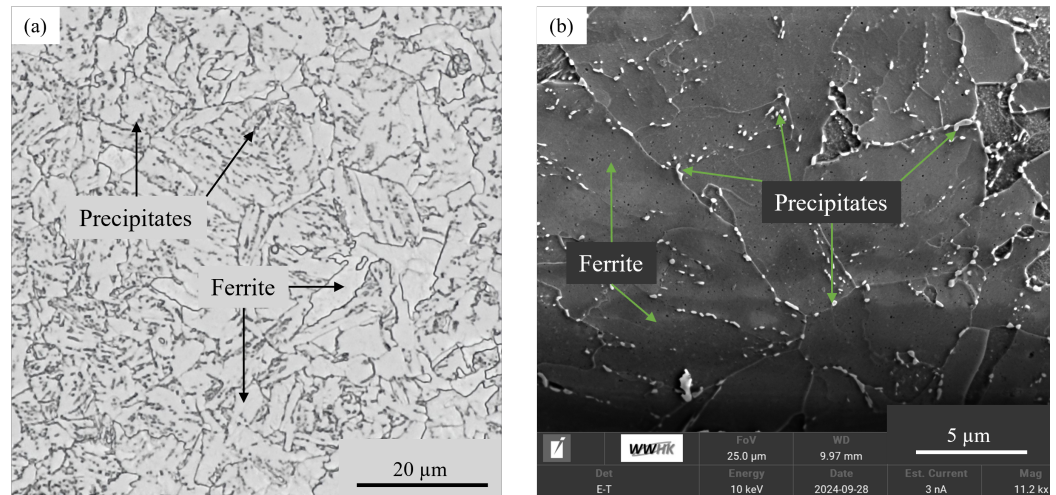
Figure 2. Microstructural analysis of the 20MnMoNi5-5 steel: (**a**) overview of the microstructure based on digital microscopy and (**b**) detailed consideration of the microstructure based on scanning electron microscopy.

For both of the steel materials presented above, crack initiation in the high cycle fatigue (HCF) regime mostly starts from the specimen surface. In addition, both materials are characterized by a comparatively homogeneous microstructure. As the inhomogeneity of the microstructure increases, damage mechanisms can shift into the volume of the material, leading to a significant effect on the scattering of the fatigue lifetime. Consequently, additional investigations a heavy-section cast of austempered ductile iron, grade EN-GJS-1050-6 are performed. The corresponding micrographs are shown in Figure 3. More detailed information regarding the mechanical properties and manufacturing of the material are provided in the research of Weber et al. [27].
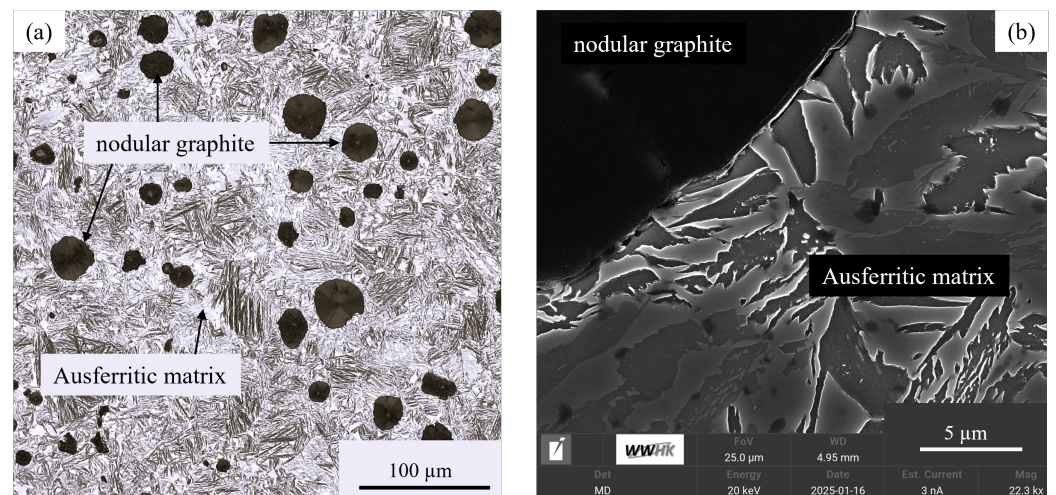

Figure 3. Microstructural analysis of the EN-GJS-1050-6 cast material: (**a**) overview of the microstructure based on digital microscopy and (**b**) detailed consideration of the microstructure based on scanning electron microscopy.

2.2. Methods

2.2.1. Experimental Setup

All fatigue tests regarding the SAE 1045 and 20MnMoNi5-5 steels were performed on a EHF-L servohydraulic testing rig from Shimadzu Deutschland GmbH (Duisburg, Germany) with a maximum load capacity of $\pm 20\,\mathrm{kN}$ and a testing frequency of 5 Hz. The the heavy-section cast specimens were tested on a MIKROTRON resonant testing rig from Russenberger Prüfmaschinen AG (Rheinfall, Switzerland) characterized by a maximum

force amplitude of $\pm 10\,\text{kN}$ and a testing frequency of 80 Hz. The specimens were loaded with a sinusoidal load–time function at ambient temperature, while the load ratio was set to $R = -1$.

The MiDAcLife (Miner Damage Accumulation Lifetime Prediction) method used in Section 3.2 to calculate virtual numbers of cycles to failure and the resulting virtual S-N curves is based on a single load increase test (LIT). In this type of fatigue test, a specimen is loaded with a load amplitude demonstrably below the fatigue strength of the material until a defined number of cycles is reached. After reaching this number of cycles, the load amplitude is increased by a certain $\Delta\sigma_a$. This process is repeated until the specimen fails, while the material response to the loading is detected using thermographic methods such as IR-thermography. Selection of the parameters for the LIT is highly dependent on the material under study and its cyclic deformation behavior. In the case of a more brittle material, the load increase must be significantly lower than for more ductile materials in order to generate a sufficient number of data points within the plastic range of the LIT. The step length is also affected by additional parameters such as the testing frequency. To consider run-up processes, the step length is increased in terms of a higher frequency. The selected areas of the stress amplitudes result from preliminary investigations of the respective materials. In addition, it should be noted that other NDT-related parameters can also be used as input for lifetime prediction testing with MiDAcLife, including electrical resistance as well as optical and magnetic properties. Within the scope of this research, a thermoIMAGER TIM QVGA-HD IR camera from Micro-Epsilon Messtechnik GmbH & Co. KG was used. Reference is made to [1,2,25], where more precise information regarding the experimental setup and measurement technologies can be found. Table 3 provides an overview regarding the experiments performed within this publication.

Table 3. Summary of the fatigue tests performed for the SAE 1045 and 20MnMoNi5-5 steel and EN-GJS-1050-6 cast iron materials.

Material	Constant Amplitude Tests	Load Increase Tests
SAE 1045	12	5
20MnMoNi5-5	21	6
EN-GJS-1050-6	14	4

2.2.2. Virtual S-N Curve Estimation According to MiDAcLife

The S-N curves presented in Section 3.2 were derived from calculations according to the MiDAcLife method, which has been used in several previous publications. The main principle of this method is that the induced partial damage D_i can be inferred from the material response measured by NDT-related techniques. The estimation of the partial damage is obtained from the correlation in Equation (9), where $\sigma_{a,\,start}$ represents the starting stress amplitude of the load increase test and $\sigma_{a,\,end}$ characterizes the last load amplitude before failure occurs. The material response is exemplified by the change in temperature, designated as $\vartheta(\sigma_a)$.

$$D_i = \frac{\int_{\sigma_{a,\,i-1}}^{\sigma_{a,\,i+1}} \vartheta(\sigma_a)\,d\sigma_a}{\int_{\sigma_{a,\,start}}^{\sigma_{a,\,end}} \vartheta(\sigma_a)\,d\sigma_a} \tag{9}$$

3. Results

3.1. Influence of the Microstructure on the Cyclic Deformation Behavior

The phenomenon of material fatigue is a complex multi-parameter process that is affected by a large number of influencing factors. In particular, the microstructural composition of a material can lead to variations in terms of the fatigue lifetime. In addition to

differences regarding the chemical composition, the type and form of precipitates are of significant importance with regard to the fatigue properties.

The LIT considered in this research can be understood as a type of 'fingerprint' of the material. In addition to the possibility of accelerated procedures for estimating the fatigue strength [2,28–32], the generated data provide insights into the cyclic deformation behavior. Based on the material's response to dynamic loading, conclusions can be drawn about whether the material exhibits relatively more brittle or ductile behavior. In addition, findings from an LIT serve as an input for the MiDAcLife LPM used to generate the virtual S-N curves in Section 3.2. The results of the performed LITs are summarized in Figure 4. Based on the displayed curve progressions, the influence of microstructural variations can be demonstrably shown.
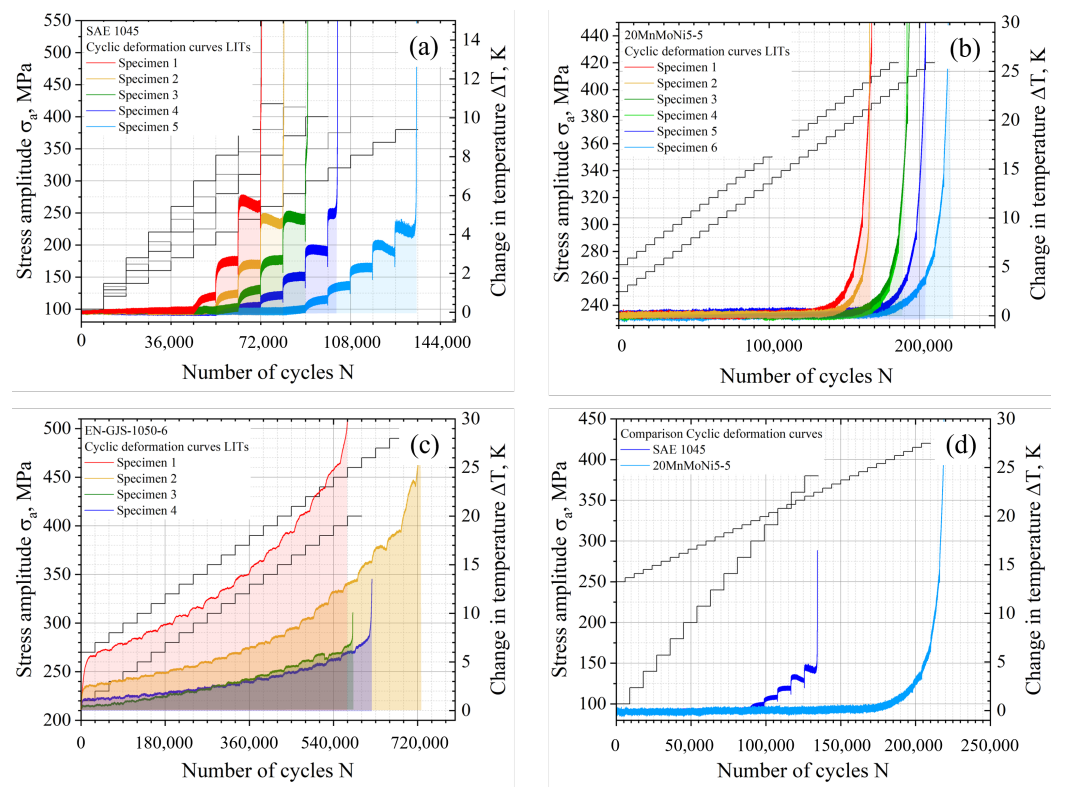

Figure 4. Investigations regarding the influence of the microstructure on the cyclic deformation behavior: (**a**) SAE 1045 steel LIT with $\sigma_{a,start} = 100\,\text{MPa}$, $\Delta\sigma_a = 20\,\text{MPa}$ and a testing frequency of $f = 5\,\text{Hz}$; (**b**) 20MnMoNi5-5 steel LIT with $\sigma_{a,start} = 250/270\,\text{MPa}$, $\Delta\sigma_a = 5\,\text{MPa}$ and a testing frequency of $f = 5\,\text{Hz}$; (**c**) EN-GJS-1050-6 LIT with $\sigma_{a,start} = 220/270\,\text{MPa}$, $\Delta\sigma_a = 10\,\text{MPa}$ and a testing frequency of $f = 80\,\text{Hz}$; (**d**) Comparison of the cyclic deformation curves regarding the steels SAE 1045 and 20MnMoNi5-5.

Because plastic deformation processes are mainly concentrated within ferritic areas, increased ductility and accordingly pronounced material response can be expected in case of the unalloyed carbon steel shown in Figure 4a. In addition to increasing progressions of the change in temperature, associated with cyclic softening processes, ranges with a decrease in the change in temperature can also be visualized. These cyclic hardening processes are attributable to dislocation reactions and reorientations within the microstructure. Compared to the findings regarding the SAE 1045 steel, the 20MnMoNi5-5 steel, which is in a quenched and tempered condition, exhibits a significantly less pronounced material response. Due to the comparatively high dislocation density resulting from the manufacturing process and the increased portion of alloying elements, a more brittle material behavior can be expected. This insight is also reflected within the curve progression of Figure 4b,

which only shows an increase of the change in temperature. Consequently, the material degradation of the 20MnMoNi5-5 steel is characterized by a purely cyclic softening.

As the investigations of the EN-GJS-1050-6 material were performed with an increased testing frequency and on a different testing rig (a MIKROTRON resonance testing rig from Russenberger Prüfmaschinen AG), these results are not directly compared with the results of the previously presented steels at this point, as increased testing frequency leads to an intensified material response. In order to enable a quantitative evaluation of the respective cyclic deformation behaviors, a new characteristic, is introduced within the context of this research in Equation (10), that is, the energy dissipation factor Φ. This integral approach defines the material response as the enclosed area of the cyclic deformation curve. To ensure the highest comparability possible of the obtained values, normalization is applied to both the corresponding number of cycles to failure N_f and the maximum value of the change in temperature ϑ_{max}, which results from frictional as well as the fracture–mechanical processes of the crack surfaces, and as such does not indicate changes within the microstructure. While the energy dissipation factor for the more brittle 20MnMoNi5-5 steel has a value of 0.016, the Φ is increased by a factor of 2.18 to $\Phi = 0.035$ in the SAE 1045 steel. This finding confirms the assumption made on the basis of Figure 4.

$$\Phi = \frac{\int_{\sigma_{a,\,start}}^{\sigma_{a,\,end}} \vartheta(\sigma_a)\,d\sigma_a}{N_f \cdot \vartheta_{max}} \tag{10}$$

3.2. Generation of Virtual S-N Curves

The generation of virtual S-N curves is based on the integration of NDT-related measurement techniques into conventional destructive materials testing. As this procedure has already been published in previous publications, reference is made to the relevant literature [1,2,25] for a more detailed explanation of MiDAcLife. To assess the quality of the lifetime prediction, the virtual S-N curves (green) in the following figures are consistently compared with conventionally determined S-N curves (black). In addition, all S-N curves include conventionally performed fatigue tests (blue) used for further validation.

The virtual S-N curve of the SAE 1045 steel illustrated in Figure 5 is characterized by precise agreement with the conventional S-N curve, with a failure probability of 50 %. While the slope is almost identical, there is only a small offset, which is negligible compared to the material-dependent scattering. Therefore, both the conventional S-N curve and the S-N curve according to MiDAcLife are very well suited to predicting conventional constant amplitude tests (CATs). The quality of the lifetime prediction is further confirmed by Figure 5b. In this illustration, both the conventionally and the virtually estimated numbers of cycles to failure are plotted against the experimental data. The precise agreement is reflected in the arrangement of the data points along the space diagonal. As a result of the homogeneous microstructure of the material, no pronounced scatter of the lifetime is observed.

Most of the same analysis from the previous evaluation can be applied to the low-alloyed 20MnMoNi5-5 steel. Comparison of the virtual S-N curve with the conventional curve from Figure 6a indicates a very high degree of correlation at this point. The scatter of the lifetime is increased compared to the unalloyed steel, especially in the range of lower stress amplitudes and for higher numbers of cycles. This can be attributed to the carbide structure within the material and the high residual compressive stresses present in the 20MnMoNi5-5 steel. Because residual stresses are superimposed with external loads, they can have a significant effect on fatigue lifetime. Despite the remarkable prediction quality shown in Figure 6b, there is a noticeable need for statistical validations of the results in terms of reliable lifetime predictions.
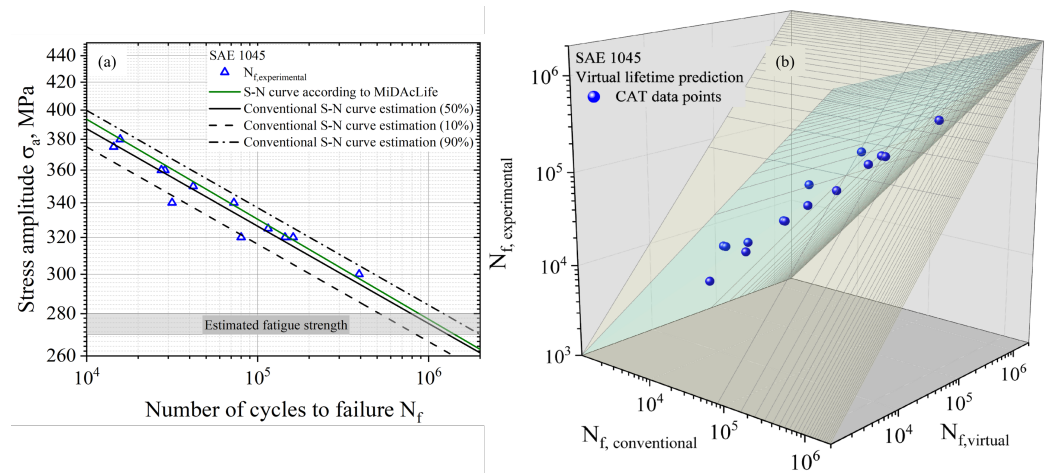
Figure 5. Generation of virtual S-N curves to estimate fatigue properties: (**a**) comparison of the virtual S-N curve according to MiDAcLife and conventionally determined S-N curves (including CATs) for validation purposes; (**b**) quality assessment of the virtually calculated data points of the SAE 1045 steel.
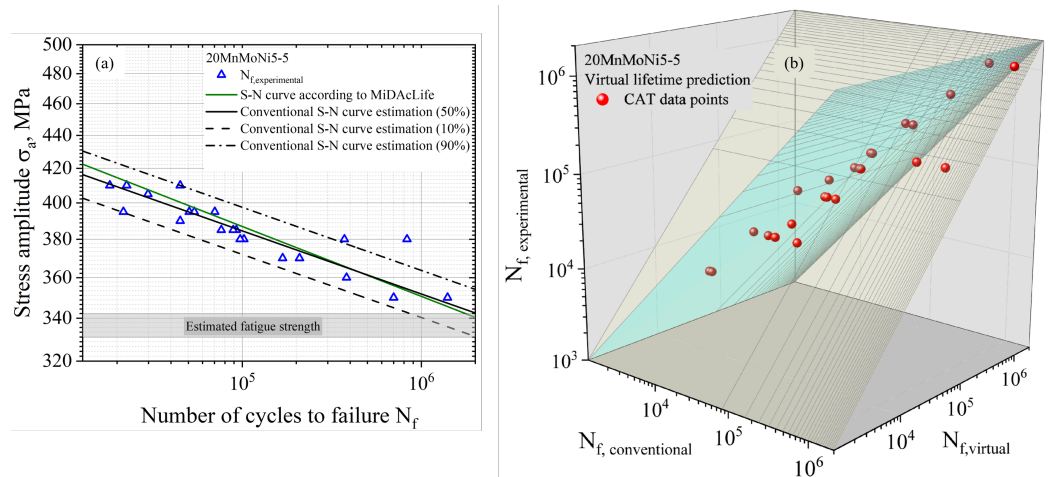

Figure 6. Generation of virtual S-N curves to estimate fatigue properties: (**a**) comparison of the virtual S-N curve according to MiDAcLife and conventionally determined S-N curves (including CATs) for validation purposes; (**b**) quality assessment of the virtually calculated data points of the 20MnMoNi5-5 steel.

The process required for statistical validation of the virtual results mentioned above is confirmed by the results of the significantly more inhomogeneous EN-GJS-1050-6, which are provided in Figure 7. Although the virtual S-N curve remains capable of describing the validation data points despite the greatly reduced number of required specimens, it is clear that further S-N curves including different failure probabilities must be estimated in order to record the increased material-dependent scattering. A detailed summary of the correlations and deviations regarding the cyclic hardening coefficient σ'_f and Basquin exponent b used to describe the S-N curve is provided at the end of this section in Table 4.
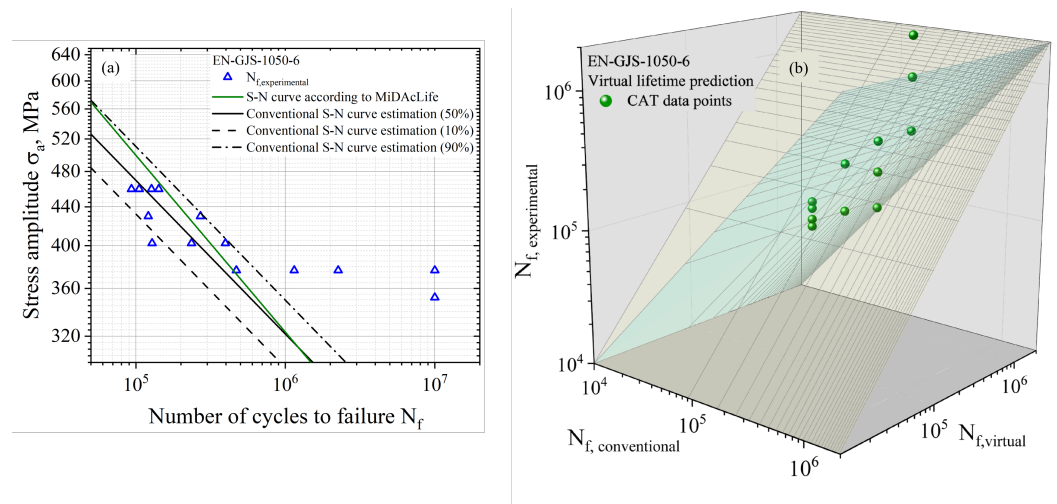
Figure 7. Generation of virtual S-N curves to estimate fatigue properties: (**a**) comparison of the virtual S-N curve according to MiDAcLife and conventionally determined S-N curves (including CATs) for validation purposes; (**b**) quality assessment of the virtually calculated data points of the EN-GJS-1050-6 cast iron

Table 4. Comparison of the S-N curve parameters regarding the SAE 1045 and 20MnMoNi5-5 steel and EN-GJS-1050 cast iron materials.

SAE 1045				
Method	σ'_f, MPa	$\delta_{\sigma'_f}$, %	b	δ_b, %
Conventional	742.1		-0.074	
MiDAcLife	793.0	6.86	-0.076	2.70
20MnMoNi5-5				
Method	σ'_f, MPa	$\delta_{\sigma'_f}$, %	b	δ_b, %
Conventional	617.2		-0.041	
MiDAcLife	633.4	2.63	-0.043	4.88
EN-GJS-1050-6				
Method	σ'_f, MPa	$\delta_{\sigma'_f}$, %	b	δ_b, %
Conventional	3114		-0.164	
MiDAcLife	4402	41.36	-0.186	13.41

3.3. Estimation of Lifetime Prediction Bands

The aim of this section is to determine virtual lifetime prediction bands (green). Analogously to conventional scatter bands (black), these enable lifetime prediction with regard to different failure probabilities. Although the presented results only refer to failure probabilities of 10%, 50%, and 90%, it should be mentioned that any other failure probability could be considered within the proposed method as well. For the previously presented results, the following illustrations contain the S-N curves of each material as well as a quality assessment of the estimation in which the virtual data points are compared with conventionally determined results. In contrast to those in the prior sections, Figures 8–10 contain both the validation tests and the virtually determined numbers of cycles to failure, which are used to calculate the lifetime prediction bands.

It should be noted that a simplification is made in developing the methodology, as the application of the pearl string method assumes that the material scattering is independent of the corresponding stress amplitude. It is especially necessary to take this simplification into

account for the EN-GJS-1050-6 cast material, and further approaches should be integrated into future developments of the proposed methodology.

To provide a sufficient database, a total of five LITs were carried out for the SAE 1045 steel material. Based on the slope of the resulting S-N curve, the virtual number of cycles to failure was transformed into a virtual load level according to the pearl string approach, which is illustrated by the filled circles. On this load level, a distribution function (log-normal distribution) can be applied to calculate the numbers of cycles to failure for defined failure probabilities. Despite the considerably reduced number of specimens, this combinatorial approach still leads to noteworthy agreement between the lifetime prediction bands and the conventional scatter bands, as can be seen in Figure 8. In addition, Figure 8b demonstrates that a major part of the data deviates from the conventional data by less than 20%, even though the experimental effort has been reduced by approximately 58%.

As a result of the combination of six LITs performed on the 20MnMoNi5-5 steel, a total of 40 virtual numbers of cycles to failure was obtained, which was then transformed into a common virtual load level according to the previous analysis shown in Figure 8. Despite the increased scatter within the lifetime, the estimated lifetime prediction bands are characterized by a high level of prediction quality. Comparison with the conventionally determined scatter bands indicates almost entirely consistent results. The arrangement of the data points within a deviation of $\pm 20\%$ in Figure 9b emphasizes the prediction quality of the virtually obtained results.
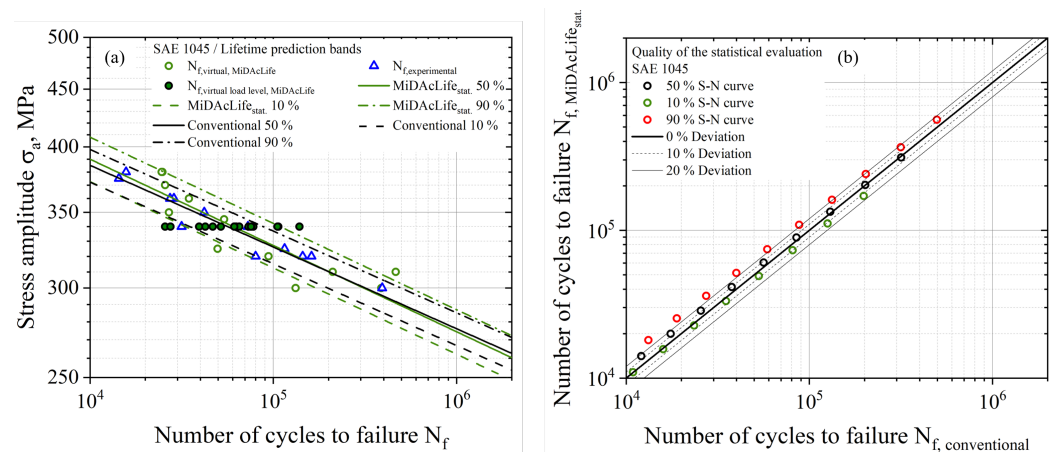

Figure 8. Generation of virtual lifetime prediction bands to describe the material-dependent scattering of the lifetime for the SAE 1045 steel: (**a**) comparison of the virtual lifetime prediction bands according to MiDAcLife and conventionally determined scatter bands (including CATs) for validation purposes; (**b**) quality assessment of the virtually calculated data points.

The conventionally performed CATs for the EN-GJS-1050-6 cast iron are shown in Figure 10. It can be seen that they are characterized by greatly increased scatter compared to previous results. This can be attributed to a number of factors, including shrinkages and the fact that graphite precipitates contained in the ausferritic matrix are subject to statistical deviations. In contrast, the S-N curves displayed in Figures 8–10 include virtual data points for two different damage sums ($D = 1$ and $D = 0.4$). Because the increased defect density leads to a reduced lifetime, the assumption of a damage sum $D = 1$ is idealized and leads to overestimation of the fatigue lifetime, which can be confirmed by the unfilled green data points in Figure 10a. This overestimation of the number of cycles to failure is particular critical with regard to safe component design. In order to consider microstructural defects specific to cast materials, Schoenborn et al. [33] examined the real damage sum of different materials. Based on these findings, they defined a maximum damage sum $D = 0.4$. The corrected results based on the adjusted damage sum are visualized by the green filled

circles in Figure 10a. As a result of the damage correction, overestimation of the lifetime can be avoided and the deviations compared to experimental validation points can be greatly reduced.
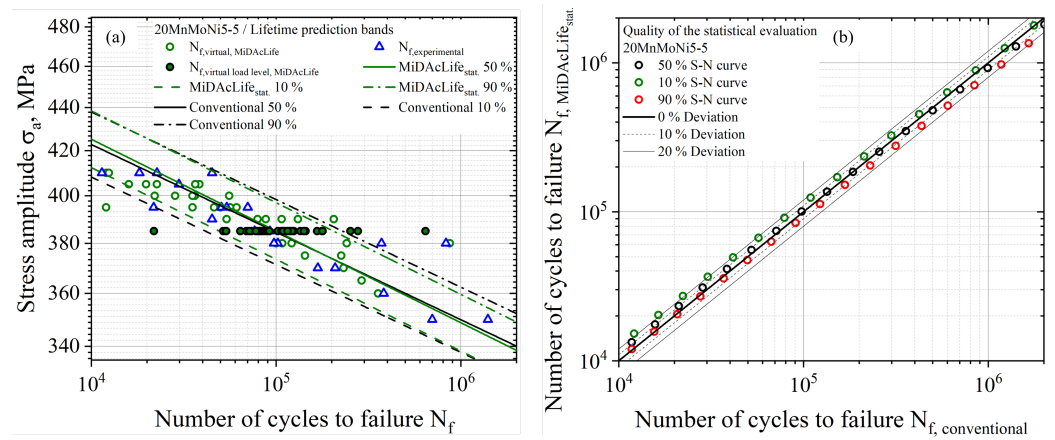

Figure 9. Generation of virtual lifetime prediction bands to describe the material-dependent scattering of the lifetime for the 20MnMoNi5-5 steel: (**a**) comparison of the virtual lifetime prediction bands according to MiDAcLife and conventionally determined scatter bands (including CATs) for validation purposes; (**b**) quality assessment of the virtually calculated data points.
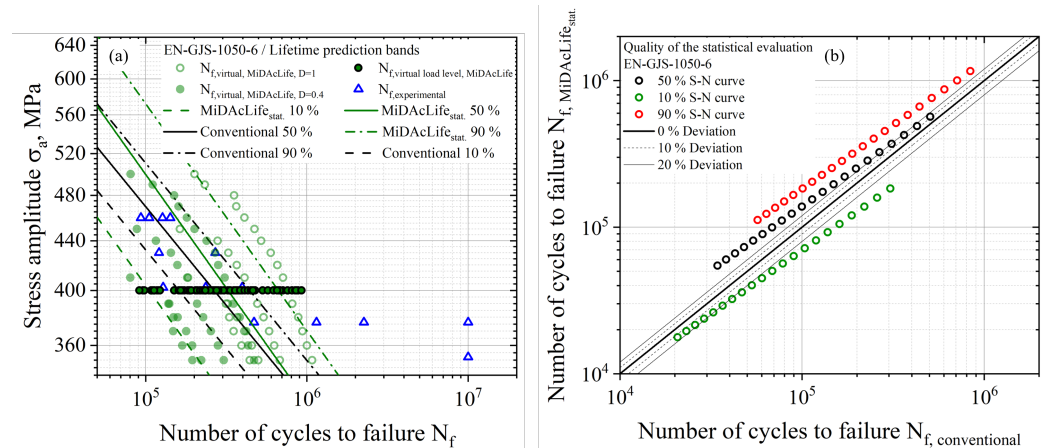

Figure 10. Generation of virtual lifetime prediction bands to describe the material-dependent scattering of the lifetime for the EN-GJS-1050-6 cast iron: (**a**) comparison of the virtual lifetime prediction bands according to MiDAcLife and conventionally determined scatter bands (including CATs) for validation purposes; (**b**) quality assessment of the virtually calculated data points.

Comparison of the virtual lifetime prediction bands with conventional results leads to the conclusion that the estimated range of scatter is too wide. This can result in over-dimensioning of components, which is contrary to lightweight construction projects aiming to achieve energy policy goals. Because a simplification is made by only considering limit values of the damage sum of 0.4 and 1, it becomes necessary to introduce the possibility of calculating a material response-related damage sum for each LIT, allowing for individualized lifetime assessments. In order to reach this goal, the energy dissipation factor is used.

By applying the Weibull distribution function (Figure 11) on the different energy dissipation factors, it is possible to determine the deviation from the maximum value of the distribution for each test. If a cyclic deformation curve of a fatigue specimen is characterized by a high energy dissipation factor, then a more significant contribution of damage has been induced, leading to a reduced lifetime; consequently, a lower damage sum must be assumed within the calculations. In contrast to this, a high damage sum needs

to be assumed in the case of a specimen with a reduced energy dissipation factor, as the induced damage is reduced. In summary, a variable, individual damage sum $D_{ind.}$ can be derived for each test as a function of the normalized material response ζ, which is provided by Equation (11).
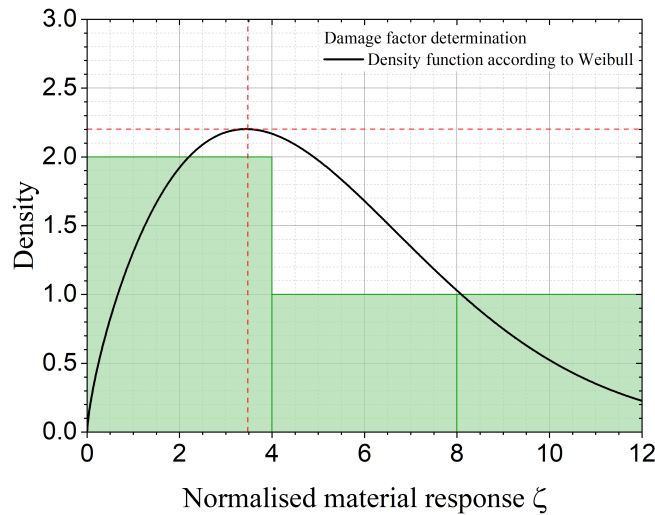

Figure 11. Variable damage factor calculation based on Weibull distribution of the energy dissipation factors of the EN-GJS-1050-6 cast iron.

$$D_{ind.} = D \cdot \frac{\zeta_{max}}{\zeta} \tag{11}$$

Based on the results in Figure 12 and the comparison of the parameters in Table 5, it can be stated that this NDT-related evaluation method enables specimen-specific variable damage assessment, leading to demonstrably improved prediction quality in terms of varying failure probabilities.
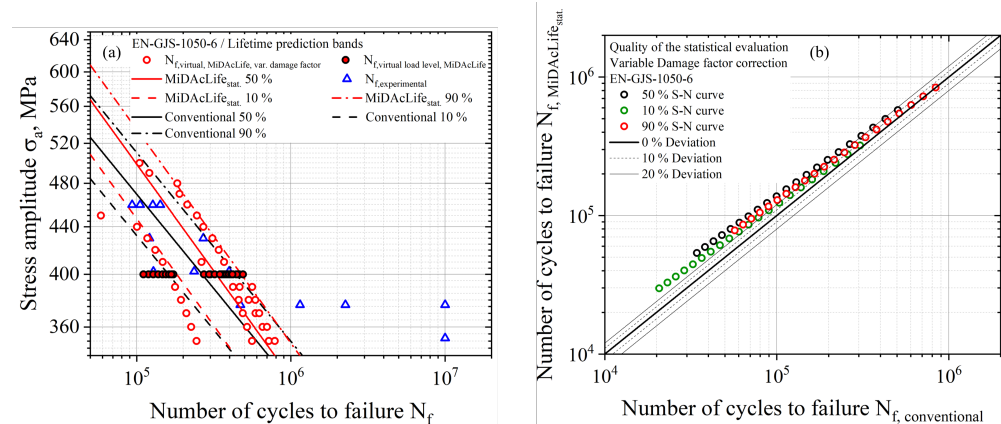

Figure 12. Generation of virtual lifetime prediction bands to describe the material-dependent scattering of the lifetime considering an individual damage sum based on the energy dissipation factor of the EN-GJS-1050-6 cast iron: (**a**) comparison of the virtual lifetime prediction bands according to MiDAcLife and conventionally determined scatter bands (including CATs) for validation purposes; (**b**) quality assessment of the virtually calculated data points.

Table 5. Comparison of the lifetime prediction curve parameters of the SAE 1045 and 20MnMoNi5-5 steel and EN-GJS-1050 cast iron materials.

Method	σ_f', MPa	$\delta_{\sigma_f'}$, %	b	δ_b, %
	SAE 1045			
Conventional 10%	742.1		−0.074	
MiDAcLife 10%	753.9	1.59	−0.076	2.70
Conventional 50%	765.9		−0.074	
MiDAcLife 50%	780.9	1.96	−0.076	2.70
Conventional 90%	791.0		−0.074	
MiDAcLife 90%	807.8	2.12	−0.076	2.70
	20MnMoNi5-5			
Conventional 10%	595.9		−0.041	
MiDAcLife 10%	612.7	2.82	−0.043	4.88
Conventional 50%	617.2		−0.041	
MiDAcLife 50%	631.8	2.37	−0.043	4.88
Conventional 90%	639.2		−0.041	
MiDAcLife 90%	651.4	1.91	−0.043	4.88
	EN-GJS-1050-6 without correction			
Conventional 10%	2867		−0.164	
MiDAcLife 10%	3558	24.10	−0.186	13.41
Conventional 50%	3114		−0.164	
MiDAcLife 50%	4402	41.36	−0.186	13.41
Conventional 90%	3385		−0.164	
MiDAcLife 90%	5041	48.92	−0.186	13.41
	EN-GJS-1050-6 with correction			
Conventional 10%	2867		−0.164	
MiDAcLife 10%	3806	32.75	−0.186	13.41
Conventional 50%	3114		−0.164	
MiDAcLife 50%	4246	36.35	−0.186	13.41
Conventional 90%	3385		−0.164	
MiDAcLife 90%	4552	34.48	−0.186	13.41

4. Discussion

Section 3.1 has addressed the influence of the microstructure on the cyclic deformation curves of different materials. The generated data originate from load increase tests conducted to characterize the cyclic deformation behavior of the materials and enable accelerated estimation of the fatigue strength. Table 6 provides an overview of the estimated fatigue strength values. To assess the quality of the fatigue strength predictions, a comparison with conventionally and virtually calculated data from Figures 5–7 is presented.

In particular, the correlation between the virtually determined data according to the MiDAcLife lifetime prediction method and the conventional data provides a precise agreement of the estimated fatigue strength. At this point it should be noted, that a limit cycle number of $N = 2 \times 10^6$ is assumed in order to ensure the highest possible comparability. Thus, further investigations to integrate the knee-point of the S-N curve are an essential part of future research.

Evaluations of the fatigue strengths of different materials based on LITs must be divided into two steps. When comparing the SAE 1045 and 20MnMoNi5-5 steels, it can be stated that the unalloyed steel shows improved prediction quality compared to the low-alloyed steel, with respective deviations of 6.130% and 9.145%. This can be explained by the methodology used in estimating the fatigue strength as well as to differences in material behavior. While a more detailed description can be found in literature [2], Figure 13 illustrates the procedure using the example of the SAE 1045 steel.

Table 6. Comparison of fatigue strength estimation regarding the SAE 1045 and 20MnMoNi5-5 steel and EN-GJS-1050 cast iron materials.

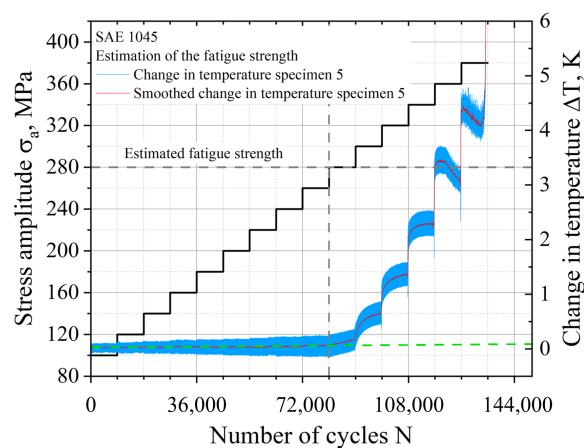| SAE 1045 N		
Method	σ_e, MPa	δ_{σ_e}, %
Conventional	261.0	
MiDAcLife	263.0	0.77
LIT	277.0	6.13
20MnMoNi5-5		
Method	σ_e, MPa	δ_{σ_e}, %
Conventional	339.0	
MiDAcLife	340.0	0.29
LIT	370.0	9.15
EN-GJS-1050-6		
Method	σ_e, MPa	δ_{σ_e}, %
Conventional	287.0	
MiDAcLife	285.0	0.70
LIT	338.0	15.09

Figure 13. Methodology for accelerated fatigue strength estimation using the example of SAE 1045 steel.

To estimate the fatigue strength, the deviation of the material's response from an initially linear correlation (green dashed line) is determined. In the case of Figure 13, an initial nonlinear material response can be observed at a stress amplitude of 280 MPa (indicated as black dashed line). All the LIT data in Table 6 result from a mean value consideration of the performed LITs.

The accuracy of the estimation can be increased with increased material response. Figure 4b shows that the increase in the material response is evidently less pronounced in case of the 20MnMoNi5-5 steel compared with the SAE 1045 steel. As a consequence,

precise determination of the first nonlinear material response is demonstrably more challenging, and cou lead to greater deviations. However, deviation of the fatigue strength of less than 10% in the context of accelerated estimation based on only one specimen is an acceptable result.

Contrary to the previous discussion, the value for the EN-GJS-1050-6 material is characterized by increased deviation. However, it must be noted that the estimated fatigue strength of the LITs fits the experimental data from Figure 7a significantly better, as run-aways have already been observed at a stress amplitude of 376 MPa. Furthermore, cast irons are generally characterized by increased scattering as a result of their microstructure.

An additional important aspect for further research following from Section 3.1 is the introduction of the energy dissipation factor Φ. It is striking that the dissipated energy increases by a factor of approximately two. This factor roughly corresponds to the variation in the carbon content of both materials. Consequently, further research should focus on the influence of carbon content, additional alloying elements, heat treatments, and further factors towards the aim individualized S-N curve generation.

In Section 3.2, the main focus is on generating virtual S-N curves from the data of only one LIT. The results are evaluated through comparison with conventional data, as summarized in Table 4. Both steels exhibit demonstrably low deviation (less than 10%) from the conventionally determined values. Considering a specimen reduction of approximately 58% in case of the SAE 1045 steel and 71% for the 20MnMoNi5-5 steel, these results highlight the potential of accelerated virtual lifetime prediction. Although the deviations of the parameters of the EN-GJS-1050-6 are characterized by increased values, the quality of the prediction can still be emphasized when taking into account the wide range of scatter in terms of the cast material.

A similar approach is taken in Table 5, where the parameters of the virtually calculated lifetime prediction bands are compared to those of the conventionally determined scatter bands. In addition to the small deviations regarding the two steels, the prediction quality for the EN-GJS-1050-6 cast iron material could be further improved as a result of the correction calculation based on the energy dissipation factor.

5. Conclusions

To account for the scatter in fatigue life due to material inhomogeneities, this research proposes an approach incorporating the MiDAcLife lifetime prediction method for different materials. An unalloyed SAE 1045 steel, an alloyed 20MnMoNi5-5 steel, and an EN-GJS-1050-6 austempered ductile cast iron were investigated. The material selection and resulting distinguishing microstructural features allow for different damage mechanisms to be taken into account. While crack initiation in terms of steels in the high cycle fatigue regime usually occurs at the surface of a specimen, cast materials are characterized by crack initiation at defects within the volume of the material. In summary, the following findings can be derived from the presented results:

- For both the SAE 1045 and 20MnMoNi5-5 steels, so-called lifetime prediction bands can be estimated despite the greatly reduced number of specimens and tests, resulting in S-N curves representing different failure probabilities
- A comparison of the virtually determined lifetime prediction bands with conventionally determined scatter bands highlights the potential of the presented method.
- To account for the evidently increased scatter of the EN-GJS-1050-6 material, in this research a new parameter called the energy dissipation factor and a method based on the in situ-measured material response is presented.
- The proposed energy dissipation factor enables specific correction of the virtual data depending on the corresponding degradation process.

- Based on the virtual lifetime prediction and the newly introduced energy dissipation factor, important approaches regarding the integration of statistical approaches into accelerated lifetime predictions were presented.

In future research, further statistical methods will be investigated and integrated into the proposed approach. Hypothesis tests appear to be a particularly promising approach for assessing the quality of the virtual lifetime prediction. In addition, the findings presented here will be extended to additional materials and material groups. Due to the increasing importance of additively manufactured materials, the presented methodology will be applied to this class of materials in future research. By varying parameters in the manufacturing process, it can be expected that it will be possible to deliberately simulate certain defect structures in order to validate the obtained results.

Author Contributions: Conceptualization, F.W. (Fabian Weber); methodology, F.W. (Fabian Weber); validation, F.W. (Fabian Weber) and F.W. (Felix Weber); formal analysis, F.W. (Fabian Weber); investigation, F.W. (Fabian Weber), J.K. and A.W.; resources, C.B. and P.S.; data curation, F.W. (Fabian Weber); writing—original draft preparation, F.W. (Fabian Weber); writing—review and editing,F.W. (Felix Weber), A.W., J.K., C.B. and P.S.; visualization, F.W. (Fabian Weber); supervision, C.B. and P.S.; project administration, F.W. (Fabian Weber); funding acquisition, C.B. and P.S. All authors have read and agreed to the published version of the manuscript.

Data Availability Statement: The raw data supporting the conclusions of this article will be made available by the authors on request.

Conflicts of Interest: The authors declare no conflicts of interest.

Abbreviations

The following abbreviations are used in this manuscript:

CAT	Constant Amplitude Test
HCF	High Cycle Fatigue
LIT	Load Increase Test
LPM	Lifetime Prediction Method
MiDAcLife	Miner Damage Accumulation Lifetime Prediction
NDT	Non-Destructive Testing
P-S-N	Fatigue Probabilistic S-N curve

Symbols

The following symbols are used in this manuscript:

D_i	Partial damage
N_f	Number of cycles to failure
n_i	Number of applied load cycles
D	Total damage sum
σ_a	Stress amplitude
σ_e	Fatigue limit
k	Slope S-N curve
$N_{fictitious}$	Fictitious number of cycles to failure
$D_{N_f - 1}$	Critical cumulative damage after reaching $N_f - 1$ cycles
Σ_i^{eq}	Stress amplitude at the ith load level (Crossland)
τ_u	Ultimate stress in torsion
$\sigma_{eq}^{i,max}$	Maximum equivalent stress
R_e	Yield strength
R_m	Tensile strength
A_t	Total elongation
$\Delta\sigma_a$	Load increase (LIT)
$\sigma_{a,start}$	Starting stress amplitude (LIT)
$\sigma_{a,end}$	Last load level before failure (LIT)
$\vartheta(\sigma_a)$	Change in temperature as a function of the stress amplitude
Φ	Energy dissipation factor
σ_f'	Cyclic hardening coefficient
b	Basquin exponent
ζ	Normalized material response
ζ_{max}	Maximum value of distribution regarding the normalized material response
δ_i	Deviation

References

1. Weber, F.; Wu, H.; Starke, P. A new short-time procedure for fatigue life evaluation based on the linear damage accumulation by Palmgren–Miner. *Int. J. Fatigue* **2023**, *172*, 107653. [CrossRef]
2. Weber, F.; Maul, M.; Juner, F.; Starke, P. A nonlinear lifetime prediction method for un- and low alloyed steels by damage determination based on non-destructive measurement techniques. *Fatigue Fract. Eng. Mater. Struct.* **2024**, *47*, 1566–1583. [CrossRef]
3. Palmgren, A. Die Lebensdauer von Kugellagern (in german). *Verein Deutscher Ingenieure* **1924**, *68*, 339–341.
4. Miner, M. Cumulative Damage in Fatigue. *J. Appl. Mech.* **1945**, *3*, 159–164. [CrossRef]
5. Bešter, T.; Fajdiga, M.; Nagode, M. Application of Constant Amplitude Dynamic Tests for Life Prediction of Air Springs at Various Control Parameters. *Stroj. Vestn.—J. Mech. Eng.* **2014**, *60*, 241–249. [CrossRef]
6. Haibach, E. *Betriebsfestigkeit*, 3rd ed.; Springer: Berlin/Heidelberg, Germany, 2006. [CrossRef]
7. Duyi, Y. A new approach to low-cycle fatigue damage based on exhaustion of static toughness and dissipation of cyclic plastic strain energy during fatigue. *Int. J. Fatigue* **2001**, *23*, 679–687. [CrossRef]
8. Manson, S.S.; Halford, G.R. Practical implementation of the double linear damage rule and damage curve approach for treating cumulative fatigue damage. *Int. J. Fract.* **1981**, *17*, 169–192. [CrossRef]
9. Benkabouche, S.; Guechichi, H.; Amrouche, A.; Benkhettab, M. A modified nonlinear fatigue damage accumulation model under multiaxial variable amplitude loading. *Int. J. Mech. Sci.* **2015**, *100*, 180–194. [CrossRef]
10. Mesmacque, G.; Garcia, S.; Amrouche, A.; Rubio-gonzalez, C. Sequential law in multiaxial fatigue, a new damage indicator. *Int. J. Fatigue* **2005**, *27*, 461–467. [CrossRef]
11. Yu, A.; Huang, H.; Li, Y.; Yang, W.; Deng, Z. A modified nonlinear fatigue damage accumulation model for life prediction of rolling bearing under variable loading conditions. *Fatigue Fract. Eng. Mater. Struct.* **2022**, *45*, 852–864. [CrossRef]
12. Aeran, A.; Siriwardane, S.; Mikkelsen, O.; Langen, I. A new nonlinear fatigue damage model based only on S-N curve parameters. *Int. J. Fatigue* **2017**, *103*, 327–341. [CrossRef]
13. Bjørheim, F.; Pavlou, D.; Siriwardane, S. Nonlinear fatigue life prediction model based on the theory of the S-N fatigue damage envelope. *Fatigue Fract. Eng. Mater. Struct.* **2022**, *45*, 1480–1493. [CrossRef]

14. Ling, J.; Pan, J. A maximum likelihood method for estimating P-S-N curves. *Int. J. Fatigue* **1997**, *19*, 415–419. [CrossRef]

15. Goglio, L.; Rossetto, M. Comparison of fatigue data using the maximum likelihood method. *Eng. Fract. Mech.* **2004**, *71*, 725–736. [CrossRef]

16. Feng, H.; Wang, Y.; Jiang, X. A Maximum Likelihood Method for Estimating Probabilistic Strain Amplitude-Fatigue Life Curves. *Acta Mech. Solida Sin.* **2018**, *31*, 80–93. [CrossRef]

17. Spindel, J.; Haibach, E. The method of maximum likelihood applied to the statistical analysis of fatigue data. *Int. J. Fatigue* **1979**, *1*. [CrossRef]

18. Tridello, A.; Boursier Niutta, C.; Rossetto, M.; Berto, F.; Paolino, D. Statistical estimation of fatigue design curves from datasets involving failures from defects. *Int. J. Fatigue* **2023**, *176*, 107882. [CrossRef]

19. Müller, C.; Wächter, M.; Masendorf, R.; Esderts, A. Distribution functions for the linear region of the S-N curve. *Mater. Test.* **2017**, *59*, 625–629. [CrossRef]

20. Schijve, J. Statistical distribution functions and fatigue of structures. *Int. J. Fatigue* **2005**, *27*, 1031–1039. [CrossRef]

21. Masendorf, R.; Müller, C. Execution and evaluation of cyclic tests at constant load amplitudes—DIN 50100:2016. *Mater. Test.* **2018**, *60*, 961–968. [CrossRef]

22. Haverkamp, K.; Forch, K. Effect of heat treatment and precipitation state on toughness of heavy section Mn-Mo-Ni-steel for nuclear power plants components. *Nucl. Eng. Des.* **1984**, *81*, 207–217. [CrossRef]

23. Das, A.; Sunil, S.; Kapoor, R. Effect of Cooling Rate on the Microstructure of a Pressure Vessel Steel. *Metallogr. Microstruct. Anal.* **2019**, *8*, 795–805. [CrossRef]

24. Gupta, L.; Maji, B.; Neogy, S.; Singh, R.; Krishnan, M. Precipitation behaviour of 20MnMoNi55 RPV steel in the temperature range of 630–670 °C. *Mater. Today Commun.* **2022**, *30*, 103096. [CrossRef]

25. Weber, F.; Starke, P. Implementation of modelled surface roughness in the accelerated lifetime prediction of a 20MnMoNi5-5 steel. *Int. J. Fatigue* **2024**, *186*, 108391. [CrossRef]

26. Teng, Z.; Wu, H.; Boller, C.; Starke, P. Thermodynamic entropy as a marker of high-cycle fatigue damage accumulation: Example for normalized SAE 1045 steel. *Fatigue Fract. Eng. Mater. Struct.* **2020**, *43*, 2854–2866. [CrossRef]

27. Weber, F.; Broeckmann, C.; Züch, V.; Jacobs, G.; Zimmermann, J.; Schröder, K.U.; Bami, Y.; Jakumeit, J.; Bodenburg, M.; Weiß, R. Multi-domain optimization of cast iron components in wind turbines. *Forsch. Ingenieurwesen* **2023**, *87*, 39–50. [CrossRef]

28. Luong, M. Infrared thermographic scanning of fatigue in metals. *Nucl. Eng. Des.* **1995**, *158*, 363–376. [CrossRef]

29. Luong, M. Nondestructive Evaluation of Fatigue Limit of Metals using Infrared Thermography. *MRS Proc.* **1997**, *503*, 275. [CrossRef]

30. Prochazka, R.; Dzugan, J.; Konopik, P. Fatigue limit evaluation of structure materials based on thermographic analysis. *Procedia Struct. Integr.* **2017**, *7*, 315–320. [CrossRef]

31. Jia, Z.; Pastor, M.L.; Garnier, C.; Gong, X. A new method for determination of fatigue limit of composite laminates based on thermographic data. *Int. J. Fatigue* **2023**, *168*, 107445. [CrossRef]

32. Guo, S.; Liu, X.; Zhang, H.; Yan, Z.; Zhang, Z.; Fang, H. Thermographic Study of AZ31B Magnesium Alloy under Cyclic Loading: Temperature Evolution Analysis and Fatigue Limit Estimation. *Materials* **2020**, *13*, 5209. [CrossRef] [PubMed]

33. Schoenborn, S.; Kaufmann, H.; Sonsino, C.; Heim, R. Cumulative Damage of High-strength Cast Iron Alloys for Automotive Applications. *Procedia Eng.* **2015**, *101*, 440–449. [CrossRef]